

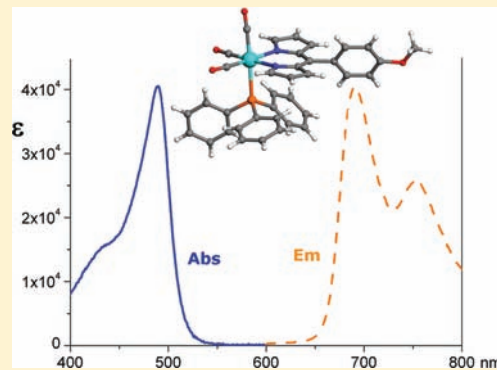
## Luminescent Rhenium(I)-Dipyrrinato Complexes

Tracey M. McLean, Janice L. Moody, Mark R. Waterland, and Shane G. Telfer\*

MacDiarmid Institute for Advanced Materials and Nanotechnology, Institute of Fundamental Sciences, Massey University, Palmerston North, New Zealand

## Supporting Information

**ABSTRACT:** The first Re(I)-dipyrrinato complexes are reported. Complexes with the general formulas  $fac\text{-}[\text{ReL}(\text{CO})_3\text{Cl}]^-$ ,  $fac\text{-}[\text{ReL}(\text{CO})_3\text{PR}_3]$ , and  $[\text{ReL}(\text{CO})_2(\text{PR}_3)(\text{PR}'_3)]$  have been prepared, where L is one of a series of *meso*-aryl dipyrrinato ligands. Access to these complexes proceeds via the reaction of  $[\text{Re}(\text{CO})_5\text{Cl}]$  with the dipyrrin (LH) to produce  $fac\text{-}[\text{ReL}(\text{CO})_3\text{Cl}]^-$ . A subsequent reaction with  $\text{PR}_3$  (R = phenyl, butyl) leads to displacement of the chloride ligand to generate  $fac\text{-}[\text{ReL}(\text{CO})_3\text{PR}_3]$ , and further reaction with  $\text{PR}'_3$  leads to the displacement of the CO ligand trans to the first  $\text{PR}_3$  ligand to give *trans*(P), *cis*(C)- $[\text{ReL}(\text{CO})_2(\text{PR}_3)(\text{PR}'_3)]$ . The structures of the complexes were determined in the solid state by X-ray crystallography and in solution by  $^1\text{H}$  NMR spectroscopy. Electronic absorption spectroscopy reveals a prominent band in the visible region at relatively low energy (472–491 nm) for all complexes, which is assigned as a  $\pi\text{-}\pi^*$  transition of the dipyrrin chromophore. Weak emission ( $\lambda_{\text{ex}} = 485$  nm, quantum yields  $<0.01$ ) was observed for  $[\text{ReL}(\text{CO})_3\text{Cl}]^-$  and  $[\text{ReL}(\text{CO})_3\text{PR}_3]$  complexes, but no emission was generally evident from the  $[\text{ReL}(\text{CO})_2(\text{PR}_3)(\text{PR}'_3)]$  complexes. On the basis of the large Stokes shift ( $\sim 6000\text{ cm}^{-1}$ ), the emission is ascribed to phosphorescence from a triplet excited state. The emission intensity is sensitive to dissolved oxygen and methyl viologen; a Stern–Volmer plot in the latter case gave a straight line. Photochemical ligand substitution reactions of  $[\text{ReL}(\text{CO})_3\text{PR}_3]$  were induced by excitation with a 355 nm laser in acetonitrile.  $[\text{ReL}(\text{CO})_2(\text{PR}_3)(\text{CH}_3\text{CN})]$  is formed as a putative intermediate, which reacts thermally with added  $\text{PR}'_3$  to produce  $[\text{ReL}(\text{CO})_2(\text{PR}_3)(\text{PR}'_3)]$  complexes.



## INTRODUCTION

The coordination chemistry of dipyrrinato ligands continues to be a very active field of research.<sup>1</sup> Dipyrrins can be viewed as “half-porphyrins”, and their conjugated  $\pi$  system gives rise to intense absorption bands in the visible region of the spectrum. Our group is particularly interested in the ability of the dipyrrin chromophores in these complexes to harvest solar radiation.<sup>2</sup> Photoluminescence is occasionally observed in dipyrrinato transition metal complexes<sup>1d,2a,3</sup> and frequently seen in  $\text{BF}_2$ -dipyrrinato compounds (BODIPYs).<sup>4</sup> The excited state responsible for luminescence is a  $\pi\text{-}\pi^*$  state that is located predominantly on the bispyrrolic core of the dipyrrin.

Since certain rhenium(I) complexes are capable of the photocatalytic reduction of  $\text{CO}_2$ <sup>5</sup> and often display other interesting photophysical properties, such as intense luminescence,<sup>6</sup> we considered that the incorporation of dipyrrin chromophores into rhenium(I) complexes would be a promising avenue for exploration. The photophysical and photochemical properties of rhenium(I) complexes may potentially be enhanced by the coordinated dipyrrinato ligands acting as light harvesting units.<sup>7</sup> This paper details the synthesis, structural characterization, and spectroscopic properties of a series of rhenium(I) complexes with dipyrrinato ligands. To the best of our knowledge, this is the first report of dipyrrinato rhenium complexes; however, a (nonemissive) azadipyrrinato complex has recently been reported.<sup>8</sup>

## EXPERIMENTAL SECTION

General synthesis conditions are summarized below. Full experimental details, including all characterization data, can be found in the Supporting Information.

**Synthesis of  $[\text{HNet}_3][\text{ReL}^A(\text{CO})_3\text{Cl}]$ .**  $\text{Re}(\text{CO})_5\text{Cl}$  and  $\text{L}^A\text{H}$  (1 equiv) were dissolved in dry toluene and heated to 100 °C. Dry triethylamine ( $\sim 2$  equiv) was then added and heating was continued for 1 h. All volatiles were then removed under reduced pressure, and the product was obtained as a crystalline orange solid by recrystallization of the residue from hot hexane/ $\text{CH}_2\text{Cl}_2$ .

**General Synthesis of  $[\text{ReL}(\text{CO})_3\text{PR}_3]$  Complexes (2A–F).** *Method 2a, Conventional Heating.*  $\text{Re}(\text{CO})_5\text{Cl}$  and LH (1 equiv) were dissolved in dry toluene and heated to 100 °C under argon. Dry triethylamine ( $\sim 2$  equiv) was added and heating continued for 1 h.  $\text{PR}_3$  (1 equiv) was then added and heating continued for a further 1 h. All volatiles were then removed under reduced pressure, and the product was obtained as a crystalline orange solid by chromatography.

*Method 2b, Microwave Heating.*  $\text{Re}(\text{CO})_5\text{Cl}$  and LH (1.25 equiv) were dissolved in dry toluene. Dry triethylamine ( $\sim 2$  equiv) was added, and the reaction was heated to 100 °C using microwave irradiation for 15 min under argon at atmospheric pressure.  $\text{PR}_3$  ( $\text{PPh}_3$  or  $\text{P}(n\text{-Bu})_3$ , 1 equiv) was then added and heating was continued for a further 15 min. All volatiles were then removed under reduced

Received: August 27, 2011

Published: November 30, 2011

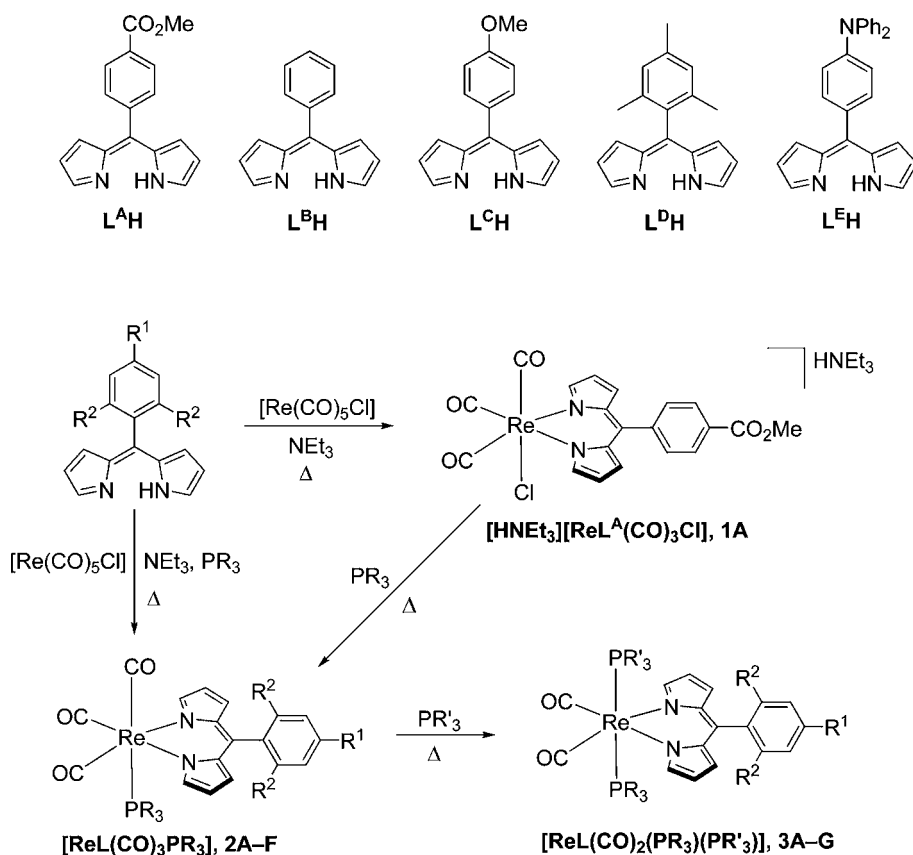


**Figure 1.** Structures of ligands  $L^A$ – $E^H$  and synthetic routes to complexes **1A**, **2A–F**, and **3A–G**.

pressure, and the product was obtained as a crystalline orange solid by chromatography.

**General Synthesis of  $[\text{ReL}(\text{CO})_2(\text{PR}_3)(\text{PR}'_3)]$  Complexes (**3A–G**).** *Method 3a, Conventional Heating.*  $[\text{ReL}(\text{CO})_3\text{PR}_3]$  and  $\text{PR}'_3$  ( $\text{PPh}_3$  or  $\text{P}(n\text{-Bu})_3$ ,  $\sim 2.5$  equiv) were combined in dry toluene and heated to  $100^\circ\text{C}$  for  $\sim 48$  h. All volatiles were then removed under reduced pressure, and the product was obtained as a crystalline orange solid by chromatography.

*Method 3b, Microwave Heating.*  $[\text{ReL}(\text{CO})_3\text{PR}_3]$  and  $\text{PR}'_3$  ( $\text{PPh}_3$  or  $\text{P}(n\text{-Bu})_3$ ,  $\sim 5.5$  equiv) were combined in dry toluene and heated to  $130^\circ\text{C}$  for 45 min using microwave irradiation (closed vessel). All volatiles were then removed under reduced pressure, and the product was obtained as a crystalline orange solid by chromatography.

**X-ray Crystallography.** Crystals suitable for X-ray crystallography were grown either from diffusion of hexane or pentane vapors into solutions of the complexes in  $\text{CH}_2\text{Cl}_2$  or  $\text{CHCl}_3$ , or by the slow evaporation of solutions of the complexes in  $\text{CH}_3\text{CN}/\text{H}_2\text{O}$ .

**1A:**  $\text{C}_{26}\text{H}_{29}\text{ClN}_3\text{O}_3\text{Re}$  ( $M_w = 685.17$ ),  $T = 123(1)$  K, triclinic, space group  $\overline{P}1$ ,  $a = 13.3468(8)$  Å,  $b = 13.6931(6)$  Å,  $c = 17.8206(9)$  Å,  $\alpha = 109.901(3)^\circ$ ,  $\beta = 90.817(4)^\circ$ ,  $\gamma = 113.659(2)^\circ$ ,  $V = 2761.6(2)$  Å<sup>3</sup>,  $Z = 4$ ,  $D_{\text{calcd}} = 1.65$  g cm<sup>-3</sup>,  $\mu = 9.85$  mm<sup>-1</sup>, 35725 measured reflections, 9252 unique reflections ( $R_{\text{int}} = 0.081$ ),  $R_1 = 0.0505$  for 7191 observed reflections ( $I > 2\sigma(I)$ ) and 658 parameters. CCDC 760501.

**2A:**  $\text{C}_{38}\text{H}_{28}\text{N}_2\text{O}_3\text{PRe}$  ( $M_w = 809.76$ ),  $T = 292(1)$  K, triclinic, space group  $\overline{P}1$ ,  $a = 9.65465(21)$  Å,  $b = 10.41243(20)$  Å,  $c = 17.73433(35)$  Å,  $\alpha = 102.480(1)^\circ$ ,  $\beta = 105.703(1)^\circ$ ,  $\gamma = 93.887(1)^\circ$ ,  $V = 1660.52(6)$  Å<sup>3</sup>,  $Z = 2$ ,  $D_{\text{calcd}} = 1.62$  g cm<sup>-3</sup>,  $\mu = 8.00$  mm<sup>-1</sup>, 22233 measured reflections, 5831 unique reflections ( $R_{\text{int}} = 0.027$ ),  $R_1 = 0.0247$  for 5552 observed reflections ( $I > 2\sigma(I)$ ) and 425 parameters. Data were collected at 292 K as the crystals were prone to disintegration at lower temperatures. CCDC 760502.

**2B:**  $\text{C}_{36}\text{H}_{26}\text{N}_2\text{O}_3\text{PRe}$  ( $M_w = 751.76$ ),  $T = 123(2)$  K, monoclinic, space group  $Cc$ ,  $a = 25.1498(5)$  Å,  $b = 8.3542(2)$  Å,  $c = 17.5653(12)$  Å,  $\beta = 128.178(9)^\circ$ ,  $V = 2901.1$  Å<sup>3</sup>,  $Z = 4$ ,  $D_{\text{calcd}} = 1.72$  g cm<sup>-3</sup>,  $\mu = 9.044$  mm<sup>-1</sup>, 17038 measured reflections, 3743 unique reflections ( $R_{\text{int}}$

$= 0.036$ ),  $R_1 = 0.023$  for 3608 observed reflections ( $I > 2\sigma(I)$ ) and 388 parameters. CCDC 837651.

**2C:**  $\text{C}_{37}\text{H}_{28}\text{N}_2\text{O}_4\text{PRe}$  ( $M_w = 781.78$ ),  $T = 292(2)$  K, triclinic, space group  $\overline{P}1$ ,  $a = 9.5888(2)$  Å,  $b = 10.3564(2)$  Å,  $c = 17.1241(12)$  Å,  $\alpha = 77.631(5)^\circ$ ,  $\beta = 75.249(5)^\circ$ ,  $\gamma = 86.802(6)^\circ$ ,  $V = 1606.30(12)$  Å<sup>3</sup>,  $Z = 2$ ,  $D_{\text{calcd}} = 1.62$  g cm<sup>-3</sup>,  $\mu = 8.22$  mm<sup>-1</sup>, 20807 measured reflections, 6005 unique reflections ( $R_{\text{int}} = 0.037$ ),  $R_1 = 0.041$  for 5363 observed reflections ( $I > 2\sigma(I)$ ) and 407 parameters. CCDC 837652.

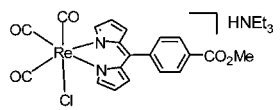
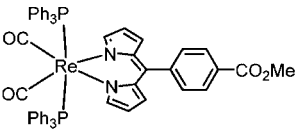
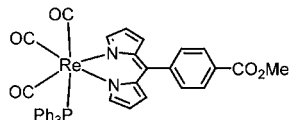
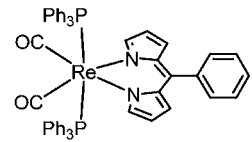
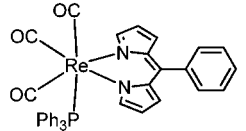
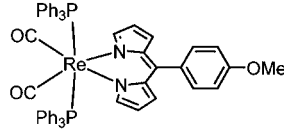
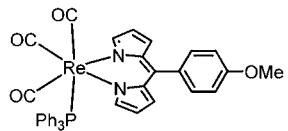
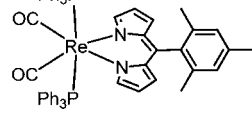
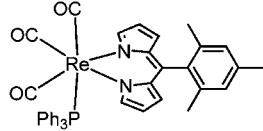
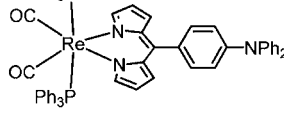
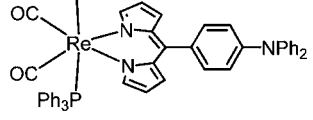
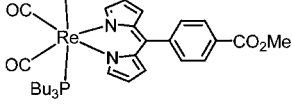
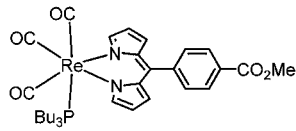
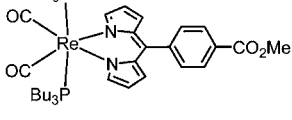
**2D:**  $\text{C}_{39}\text{H}_{32}\text{N}_2\text{O}_3\text{PRe}$  ( $M_w = 793.84$ ),  $T = 123(2)$  K, orthorhombic, space group  $Pbca$ ,  $a = 16.966(3)$  Å,  $b = 17.746(4)$  Å,  $c = 21.892(4)$  Å,  $V = 6591(2)$  Å<sup>3</sup>,  $Z = 8$ ,  $D_{\text{calcd}} = 1.60$  g cm<sup>-3</sup>,  $\mu = 7.99$  mm<sup>-1</sup>, 21037 measured reflections, 4647 unique reflections ( $R_{\text{int}} = 0.074$ ),  $R_1 = 0.047$  for 4355 observed reflections ( $I > 2\sigma(I)$ ) and 417 parameters. CCDC 837653.

**2E:**  $\text{C}_{48}\text{H}_{35}\text{N}_3\text{O}_3\text{PRe}$  ( $M_w = 918.96$ ),  $T = 123(2)$  K, triclinic, space group  $\overline{P}1$ ,  $a = 9.2055(2)$  Å,  $b = 13.6362(3)$  Å,  $c = 16.0589(11)$  Å,  $\alpha = 80.409(6)^\circ$ ,  $\beta = 85.950(6)^\circ$ ,  $\gamma = 76.312(5)^\circ$ ,  $V = 1930.19(15)$  Å<sup>3</sup>,  $Z = 2$ ,  $D_{\text{calcd}} = 1.58$  g cm<sup>-3</sup>,  $\mu = 6.93$  mm<sup>-1</sup>, 27584 measured reflections, 7247 unique reflections ( $R_{\text{int}} = 0.048$ ),  $R_1 = 0.040$  for 6750 observed reflections ( $I > 2\sigma(I)$ ) and 505 parameters. CCDC 837654.

**2F:**  $\text{C}_{32}\text{H}_{40}\text{N}_2\text{O}_3\text{PRe}$  ( $M_w = 794.83$ ),  $T = 123(2)$  K, monoclinic, space group  $P2_1/c$ ,  $a = 18.6016(13)$  Å,  $b = 11.1012(6)$  Å,  $c = 15.5656(10)$  Å,  $\beta = 95.693(7)^\circ$ ,  $V = 3198.4(3)$  Å<sup>3</sup>,  $Z = 4$ ,  $D_{\text{calcd}} = 1.557$  g cm<sup>-3</sup>,  $\mu = 8.24$  mm<sup>-1</sup>, 22471 measured reflections, 5158 unique reflections ( $R_{\text{int}} = 0.080$ ),  $R_1 = 0.082$  for 3370 observed reflections ( $I > 2\sigma(I)$ ) and 344 parameters. A data cutoff of 0.865 Å was applied during the refinement because of the low intensity of the very high angle reflections. CCDC 837655.

**3A·H<sub>2</sub>O:**  $\text{C}_{55}\text{H}_{43}\text{N}_2\text{O}_4\text{P}_2\text{Re}$  ( $M_w = 1045.10$ ),  $T = 143(2)$  K, triclinic, space group  $\overline{P}1$ ,  $a = 11.9210(5)$  Å,  $b = 19.9068(6)$  Å,  $c = 21.6044(15)$  Å,  $\alpha = 99.761(7)^\circ$ ,  $\beta = 91.342(6)^\circ$ ,  $\gamma = 90.080(6)^\circ$ ,  $V = 5051.2(4)$  Å<sup>3</sup>,  $Z = 4$ ,  $D_{\text{calcd}} = 1.39$  g cm<sup>-3</sup>,  $\mu = 5.674$  mm<sup>-1</sup>, 60443 measured reflections, 18166 unique reflections ( $R_{\text{int}} = 0.11$ ).  $R_1 = 0.1233$  for 12553 observed reflections ( $I > 2\sigma(I)$ ) and 1163 parameters. CCDC 837656.

Table 1. Structures of Complexes 1A, 2A–F, and 3A–G and Reaction Yields

Structure	Yield (%)	Structure	Yield (%)
<b>1A</b> 	75	<b>3A</b> 	49
<b>2A</b> 	87	<b>3B</b> 	80
<b>2B</b> 	37	<b>3C</b> 	86
<b>2C</b> 	49	<b>3D</b> 	95
<b>2D</b> 	93	<b>3E</b> 	59
<b>2E</b> 	36	<b>3F</b> 	92
<b>2F</b> 	78	<b>3G</b> 	47

**3B**·C<sub>5</sub>H<sub>12</sub>: C<sub>58</sub>H<sub>53</sub>N<sub>2</sub>O<sub>2</sub>P<sub>2</sub>Re (*M<sub>w</sub>* = 1058.16), *T* = 123(2) K, monoclinic, space group *P*2<sub>1</sub>/*c*, *a* = 20.5988(4) Å, *b* = 12.3217(2) Å, *c* = 20.7201(15) Å, β = 115.655(8)°, *V* = 4720.2(4) Å<sup>3</sup>, *Z* = 4, *D<sub>calcd</sub>* = 1.48 g cm<sup>-3</sup>, μ = 6.01 mm<sup>-1</sup>, 48532 measured reflections, 8905 unique reflections (*R<sub>int</sub>* = 0.066), *R*<sub>1</sub> = 0.066 for 7268 observed reflections (*I* > 2σ(*I*)) and 586 parameters. CCDC 837657.

**3C**·CHCl<sub>3</sub>: C<sub>55</sub>H<sub>44</sub>Cl<sub>3</sub>N<sub>3</sub>O<sub>3</sub>P<sub>2</sub>Re (*M<sub>w</sub>* = 1135.41), *T* = 143(2) K, monoclinic, space group *P*2<sub>1</sub>/*c*, *a* = 19.4332(4) Å, *b* = 12.2647(2) Å, *c* = 21.4332(15) Å, β = 108.448(8)°, *V* = 4845.9(4) Å<sup>3</sup>, *Z* = 4, *D<sub>calcd</sub>* = 1.56 g cm<sup>-3</sup>, μ = 7.42 mm<sup>-1</sup>, 50108 measured reflections, 9275 unique reflections (*R<sub>int</sub>* = 0.042), *R*<sub>1</sub> = 0.033 for 8281 observed reflections (*I* > 2σ(*I*)) and 596 parameters. CCDC 837658.

**3D**: C<sub>56</sub>H<sub>47</sub>N<sub>2</sub>O<sub>2</sub>P<sub>2</sub>Re (*M<sub>w</sub>* = 1028.10), *T* = 123(2) K, monoclinic, space group *P*2<sub>1</sub>/*c*, *a* = 16.470(3) Å, *b* = 13.150(2) Å, *c* = 23.440(16) Å, β = 102.34(7)°, *V* = 4949.3 Å<sup>3</sup>, *Z* = 4, *D<sub>calcd</sub>* = 1.38 g cm<sup>-3</sup>, μ = 5.73 mm<sup>-1</sup>, 28154 measured reflections, 5904 unique reflections (*R<sub>int</sub>* = 0.073), *R*<sub>1</sub> = 0.047 for 4889 observed reflections (*I* > 2σ(*I*)) and 569 parameters. A data cutoff of 0.95 Å was applied during the refinement

because of the poor agreement between *F<sub>obs</sub>* and *F<sub>calc</sub>* for many high angle reflections. CCDC 837659.

**3E**: C<sub>65</sub>H<sub>50</sub>N<sub>3</sub>O<sub>2</sub>P<sub>2</sub>Re (*M<sub>w</sub>* = 1153.22), *T* = 123(2) K, triclinic, space group *P* $\bar{1}$ , *a* = 11.9337(2) Å, *b* = 12.8775(2) Å, *c* = 17.2623(12) Å, α = 97.802(7)°, β = 90.789(6)°, γ = 98.190(7)°, *V* = 2599.96(19) Å<sup>3</sup>, *Z* = 2, *D<sub>calcd</sub>* = 1.47 g cm<sup>-3</sup>, μ = 5.54 mm<sup>-1</sup>, 36714 measured reflections, 9720 unique reflections (*R<sub>int</sub>* = 0.071), *R*<sub>1</sub> = 0.061 for 8416 observed reflections (*I* > 2σ(*I*)) and 658 parameters. CCDC 837660.

**3G**: C<sub>49</sub>H<sub>55</sub>N<sub>2</sub>O<sub>4</sub>P<sub>2</sub>Re (*M<sub>w</sub>* = 984.14), *T* = 143(2) K, monoclinic, space group *P*2<sub>1</sub>/*n*, *a* = 12.0645(2) Å, *b* = 23.9343(4) Å, *c* = 15.6919(11) Å, β = 98.539(7)°, *V* = 4480.9(3) Å<sup>3</sup>, *Z* = 4, *D<sub>calcd</sub>* = 1.46 g cm<sup>-3</sup>, μ = 6.34 mm<sup>-1</sup>, 40509 measured reflections, 6616 unique reflections (*R<sub>int</sub>* = 0.096), *R*<sub>1</sub> = 0.071 for 4857 observed reflections (*I* > 2σ(*I*)) and 514 parameters. A data cutoff of 0.87 Å was applied during the refinement because of the low intensity of the very high angle reflections. CCDC 837661.

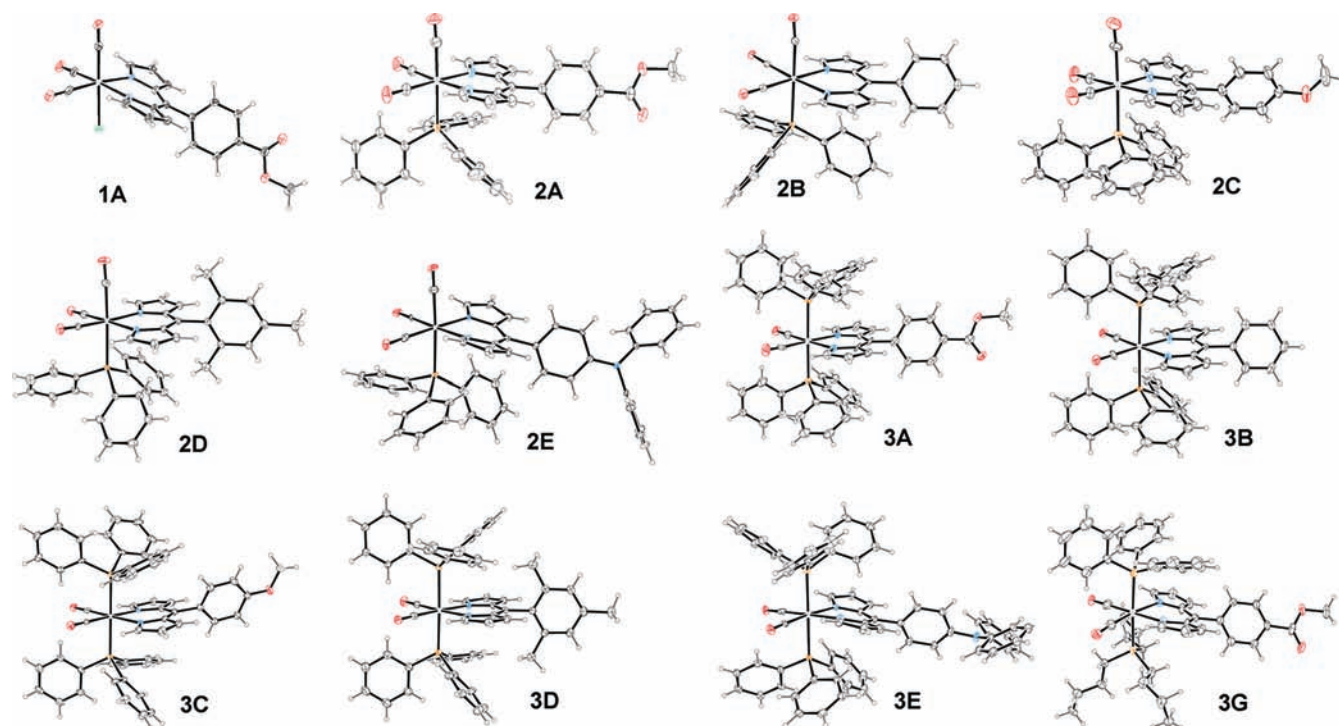


**Figure 2.** ORTEP representations (30% probability level) of the molecular structures of **1A**, **2A–E**, and **3A–E**, and **3G** as determined by X-ray crystallography. Black = C; red = O; blue = N; gray = Re; green = Cl. Hydrogen atoms are represented as unfilled spheres. The  $\text{HNEt}_3$  counterion of **1A** has been omitted for clarity.

## RESULTS AND DISCUSSION

**Synthesis.** The structures of ligands  $\text{L}^{\text{A–E}}\text{H}$  and the general synthetic routes to the three sets of complexes discussed in this work,  $[\text{HNEt}_3][\text{ReL}(\text{CO})_3\text{Cl}]$  (**1**),  $[\text{ReL}(\text{CO})_3\text{PR}_3]$  (**2**), and  $[\text{ReL}(\text{CO})_2(\text{PR}_3)(\text{PR}'_3)]$  (**3**), are depicted in Figure 1. R and R' are either phenyl or *n*-butyl.

In exploratory synthetic work, it was found that the reaction between  $[\text{Re}(\text{CO})_5\text{Cl}]$  and  $\text{L}^{\text{A}}\text{H}$  and the presence of base leads to the displacement of two CO ligands from  $[\text{Re}(\text{CO})_5\text{Cl}]$  by the deprotonated dipyrin. The reaction is regioselective, presumably because of the strong trans effect of CO ligands, and produces  $\text{fac-}[\text{HNEt}_3][\text{ReL}^{\text{A}}(\text{CO})_3\text{Cl}]$  (**1A**) as a deeply colored orange crystalline solid. Since this compound has a tendency to decompose over a few weeks at room temperature, other complexes in this family were not pursued.

An expeditious route to the family of  $[\text{ReL}(\text{CO})_3\text{PR}_3]$  complexes (**2A–F**) was developed, which relied on the in situ displacement of the chloride ligand in  $[\text{ReL}(\text{CO})_3\text{Cl}]^-$  by  $\text{PR}_3$  (R = phenyl, *n*-butyl) in hot toluene. The products, **2A–F**, are conveniently isolated as dichroic orange/green crystals, which appear to be indefinitely stable at room temperature in the dark.

The reaction of  $[\text{ReL}(\text{CO})_3\text{PR}_3]$  with further phosphine ( $\text{PR}'_3$ , R' = phenyl, *n*-butyl) results in the displacement of the CO ligand that is positioned trans to the coordinated phosphine ligand to produce the set of complexes formulated as  $[\text{ReL}(\text{CO})_2(\text{PR}_3)(\text{PR}'_3)]$  (**3A–G**). These complexes appear as red or brown solids, often crystalline. Typically,  $\text{PR}_3 = \text{PR}'_3$ ; however mixed phosphine complexes such as **3G** (Table 1) are accessible. Conducting these reactions using microwave irradiation rather than conventional heating shortened the reaction times and generally led to improved yields.

The above synthetic methodology shares many similarities with  $\text{Re}(\text{I})/2,2'$ -bipyridine chemistry.<sup>9</sup> For example, the reaction of  $[\text{Re}(\text{CO})_5\text{Cl}]$  and 2,2'-bipyridine (bipy) yields  $\text{fac-}[\text{Re}(\text{bipy})(\text{CO})_3\text{Cl}]$  and further reaction with a phosphine ligand ( $\text{PR}_3$ ) furnishes  $\text{fac-}[\text{Re}(\text{bipy})(\text{CO})_3\text{PR}_3]^+$ . This step typically employs Ag(I) to assist the displacement of the chloride ligand from  $[\text{Re}(\text{bipy})(\text{CO})_3\text{Cl}]$ ;<sup>6d,10</sup> however, this is not required for the above  $[\text{ReL}^{\text{A}}(\text{CO})_3\text{Cl}]^-$  complexes. Synthetic routes to the  $[\text{Re}(\text{bipy})(\text{CO})_2(\text{PR}_3)_2]^+$  complexes are highly varied, and both thermal and photochemical pathways have been employed from  $[\text{Re}(\text{bipy})(\text{CO})_3\text{Cl}]$ .<sup>6a,f,11</sup>

**X-ray Crystallography.** The structures of all of the complexes listed in Table 1 except **3F** (13 structures in total) were established by X-ray crystallography (Figure 2). **1A** crystallizes in the space group  $\text{P}\bar{1}$ , and the asymmetric unit features two independent copies of both  $\text{HNEt}_3^+$  and  $[\text{ReL}^{\text{A}}(\text{CO})_3\text{Cl}]^-$ . The Re center of the  $[\text{ReL}^{\text{A}}(\text{CO})_3\text{Cl}]^-$  anion adopts a distorted octahedral geometry in both cases. The three CO ligands are arranged with a *fac* geometry around the Re center with Re–C bond lengths falling between 1.876(9) and 1.927(9) Å, while the Re–Cl bond lengths are 2.5023(18) and 2.519(2) Å. The Re–N bond distances fall in the range 2.145–2.161 Å, which are slightly larger than observed for other known third-row transition metal-dipyrinato complexes that feature Ir(III)<sup>1d</sup> and Pt(II)<sup>3c</sup> but on par with a reported Re(I)-azadipyrinato complex.<sup>8</sup> The dipyrinato ligand is distinctly canted away from the equatorial plane (defined by the Re atoms and the C donor atoms of the two CO ligands trans to the  $\text{L}^{\text{A}}$ ) of both complex anions with tilt angles<sup>1d</sup> of 26.2 and 27.6°. A similar distortion has been observed in other complexes of dipyrinato and azadipyrinato ligands.<sup>1d,2a,8,12</sup> The phenyl ring of the dipyrinato ligand is approximately orthogonal to the bispyrrolic core.



The molecular structures of the  $[\text{ReL}(\text{CO})_3\text{PR}_3]$  complexes **2A–F** (Figure 2) display a distorted octahedral geometry about the Re center. Tilting of the dipyrinato chelate is less pronounced than in **1A**, with a maximum tilt angle of  $17.2^\circ$  observed for **2E**, which is probably a consequence of the steric bulk of the phosphine ligand. The Re–N bond distances (2.108–2.225 Å) are slightly larger than those for **1A**, which may be due to a stronger trans effect from the CO ligands. In general, the phenyl ring is twisted out of the plane of the dipyrin core between  $57$  and  $71^\circ$ , though in **2D** (mesityl substituent) it is essentially orthogonal. The CO ligands are in a *fac* arrangement, and the Re–C bond distances (typically 1.940–1.962 Å for the CO ligands trans to the  $\text{PPh}_3$  ligand and 1.910–1.936 Å for those trans to the dipyrinato N donor atoms, though some outliers are observed in **2D** and **2F**) reflect the relative trans effects induced by the  $\text{PPh}_3$  and dipyrinato ligands.

The X-ray crystal structures of **3A–E** and **3G** confirm the anticipated molecular structures of these complexes (Figure 2). All complexes have a distorted octahedral geometry about the Re center with the dipyrinato ligand core lying nearly in the plane defined by the Re center and the two trans CO ligands. The exceptions to this are **3E** and **3G**, where the tilt angles of the dipyrinato ligand are  $16$  and  $18^\circ$ , respectively. The angle between the mean planes of the two pyrrolic rings of the dipyrinato chelate in **3E** is  $15^\circ$ . Such deviations from planarity are well-known for this class of ligand.<sup>18,13</sup> The Re–N bond distances lie between 2.161 and 2.201 Å, which are slightly larger than those of **1A** but are comparable with those of **2A–F**. The Re–C bond distances to the CO ligands lie between 1.871 and 1.968 Å, which are comparable to those in **1A** and **2A**.

**NMR Spectroscopy.** The  $^1\text{H}$  and  $^{31}\text{P}$  NMR spectra of the *fac*- $[\text{ReL}(\text{CO})_3\text{PR}_3]$  complexes **2A–G** are consistent with their anticipated structures. With the aid of COSY NMR spectra, the aromatic peaks could be assigned. In all cases, the six pyrrolic protons  $\text{H}^{\text{a-c}}/\text{H}^{\text{a'-c'}}$  are observed in clusters: resonances corresponding to four ( $\text{H}^{\text{b/b'}}$  and  $\text{H}^{\text{c/c'}}$ ) of the six protons lie between 6.18 and 6.50 ppm and the remaining two protons ( $\text{H}^{\text{a/a'}}$ ) are located further downfield in the range 7.47–7.96 ppm. In all cases, the average  $C_2$  symmetry of the complexes is reflected by the magnetic equivalence of the  $\text{H}^{\text{a-c}}$  and  $\text{H}^{\text{a'-c'}}$  protons. Rapid rotation of the phenyl ring does not readily occur for most complexes at  $25^\circ\text{C}$  as evidenced by the four distinct doublets that are observed for  $\text{H}^{\text{d/e}}$  and  $\text{H}^{\text{d'/e'}}$  in most NMR spectra. This implies that the transannular torsion angle  $\alpha$  (Figure 3) averages  $90^\circ$ , although it likely rocks back and

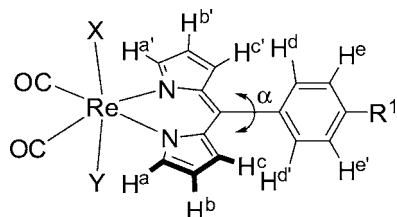


**Figure 3.** Labeling scheme used in the discussion of the  $^1\text{H}$  NMR spectra of the Re(I)-dipyrinato complexes. Note that protons  $\text{H}^{\text{d/d'}}$  are replaced by methyl groups in **2D** and **3D**.

forth about this position. The phenyl ring resonances are fairly broad for **2C** and **2E**, indicating that phenyl ring rotation occurs near the NMR time scale in these cases. This dynamic process can be frozen out at  $-10^\circ\text{C}$ , as evidenced by the

appearance of four distinct peaks (Figure 4). In **2A–C** and **2E**, one of the phenyl ring protons ( $\text{H}^{\text{d}}$  in Figure 3 where  $\text{X} =$

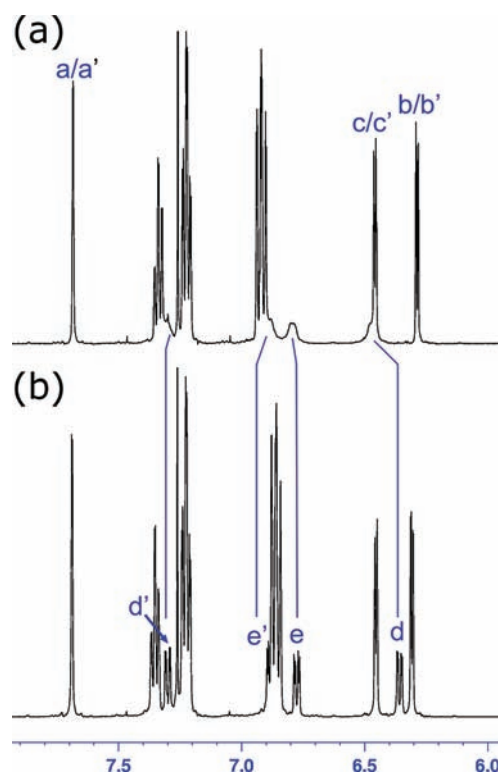


**Figure 4.** Aromatic region of the  $^1\text{H}$  NMR spectra of **2C** in  $\text{CDCl}_3$  at (a)  $25^\circ\text{C}$ ; and (b)  $-10^\circ\text{C}$ . The proton labels are given in Figure 3, where ligand  $\text{X} = \text{PPh}_3$ .

$\text{PPh}_3$ ) experiences a significant upfield shift (to  $\sim 6.26$ – $6.78$  ppm) compared to the corresponding resonances in **1A** and **2F**. This is a consequence of its proximity to the  $\pi$  clouds of the  $\text{PPh}_3$  ligand.

The  $^1\text{H}$  and  $^{31}\text{P}$  NMR spectra of the  $[\text{ReL}(\text{CO})_2(\text{PR}_3)(\text{PR}'_3)]$  complexes (**3A–G**) are consistent with their expected structures and  $C_{2h}$  point group symmetry. Complexes **3A–F** have 2-fold rotational symmetry, which renders  $\text{H}^{\text{a-c}}/\text{H}^{\text{a'-c'}}$  and  $\text{H}^{\text{d-e}}/\text{H}^{\text{d'-e'}}$  (as well as the two  $^{31}\text{P}$  nuclei) magnetically equivalent. This symmetry is lost in **3G**, which incorporates both  $\text{PPh}_3$  and  $\text{P}(n\text{-Bu})_3$  ligands, and its  $^1\text{H}$  NMR spectrum thus resembles the spectra of **2A–F** discussed above.

**Electronic and Vibrational Spectroscopy.** All complexes were further characterized in the solid state by ATR-IR spectroscopy. Three strong bands are observed in the range  $1863$ – $2004\text{ cm}^{-1}$  for **1A**, and between  $1880$  and  $2012\text{ cm}^{-1}$  for **2A–F**, which is consistent with the facial disposition of the three carbonyl ligands about a pseudo-octahedral metal center.<sup>14</sup> These vibrations can be assigned as a totally symmetric in-phase vibration  $\text{A}'(1)$ , an out-of-phase totally symmetric vibration  $\text{A}'(2)$ , and out-of-phase asymmetric vibration  $\text{A}''$ .<sup>15</sup> For complexes **3A–G**, two strong bands are observed between  $1822$  and  $1912\text{ cm}^{-1}$ , as expected for two cis-coordinated CO ligands and as seen in complexes such as  $[\text{Re}(\text{bipy})(\text{CO})_2(\text{PR}_3)_2]^+$ .<sup>6a,11a</sup> These vibrations are assigned as an out-of-phase totally symmetric vibration  $\text{A}'(2)$  and an out-of-phase asymmetric mode  $\text{A}''$ . By comparison with related complexes,<sup>2a</sup> all of the prominent peaks in the  $1727$ – $995$

$\text{cm}^{-1}$  region can be attributed to vibrational modes of the dipyrinato ligand.

The electronic absorption spectra of **1A**, **2A**, and **3A** are presented in Figure 5 as a representative selection of the

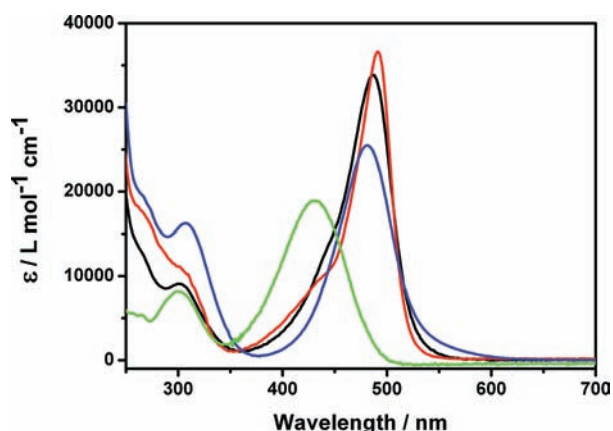


**Figure 5.** Representative absorbance spectra of each family of Re(I) dipyrinato complexes recorded in  $\text{CH}_2\text{Cl}_2$ . **1A** = black, **2A** = red, **3A** = blue. The absorption spectrum of  $\text{L}^{\text{A}}\text{H}$  in MeOH is shown for comparison (green).

complexes reported in this paper. All complexes display an intense band centered between 480–491 nm (Table 2). This band stems from an  $\text{S}_0 \rightarrow \text{S}_1$  (primarily  $\pi-\pi^*$ ) transition that is centered mainly on the dipyrinato ligand.<sup>16</sup> By comparison with other known dipyrinato complexes, it is clear that the energy of this transition is relatively insensitive to the identity of the metal ion.<sup>1a,d,2a,b,3a,e,16b,17</sup> Exciton coupling<sup>2b</sup> is not observed in these complexes since the complexes only contain a single dipyrinato ligand. In common with many other dipyrinato complexes<sup>2b,17,18</sup> and BODIPYs,<sup>19</sup> vibronic structure is often apparent as a shoulder or minor inflection on the high energy side of the dominant absorption band.

There are subtle differences in the absorption spectra of  $[\text{ReL}(\text{CO})_3\text{PR}_3]$  and  $[\text{ReL}(\text{CO})_2(\text{PR}_3)(\text{PR}'_3)]$  complexes: the absorption maxima of the dominant band are slightly blue-shifted and have a lower extinction coefficients for  $[\text{ReL}(\text{CO})_2(\text{PR}_3)(\text{PR}'_3)]$ . There is also a clear tendency for the complexes that feature  $\text{PBu}_3$  ligands (**2F**, **3F**, and **3G**) to lead to slightly blue-shifted  $\pi-\pi^*$  absorption bands with respect to their  $\text{PPh}_3$  counterparts. The absorption spectrum of **2F** parallels that of other  $[\text{ReL}(\text{CO})_3\text{PR}_3]$  complexes in terms of peak intensity although the vibronic structure is less prominent in this case (Supporting Information, Figure S1).

Minor peaks (or shoulders) are present in the absorption spectra of the complexes around 300 nm. Similar spectral features have been noted for Ir(III)-dipyrinato complexes and certain BODIPYs<sup>1d,19b</sup> in which they have been ascribed as dipyrinato-centered  $\text{S}_0 \rightarrow \text{S}_2$  transitions. A similar assignment can be made for our Re(I) complexes on the basis of excitation spectra (see below); the underlying transitions directly involve the dipyrinato chromophore. The intensity of the bands in this spectral region has previously been correlated with the ease of rotation of the phenyl substituents; hindering the rotation of the phenyl ring reduces the probability of the transition.<sup>19b</sup> However, similar correlations do not appear to exist for the complexes reported herein. The peak at 302 nm is very prominent in the absorption spectra of **2E** and **3E** (Figure 6), which may arise from supplementary transitions involving the diphenylamino substituent,<sup>20</sup> for example, contributions from intraligand charge transfer transitions involving the lone pair of the nitrogen atom.

Resonance Raman spectroscopy confirms that the dominant feature in the visible region of the absorption spectra of the complexes is localized on the dipyrinato ligand. Excitation wavelengths of 458 and 488 nm were employed, and the spectra for all the complexes are presented in the Supporting Information, Figures S3–S15. The spectra closely resemble the resonance Raman spectra of  $[\text{RuL}^{\text{A}}(\text{bipy})_2]^{+16}$  at these wavelengths. This reflects the similarity of the vibrational modes of the dipyrinato framework that are involved in

**Table 2.** Summary of the Optical Properties (in  $\text{CH}_2\text{Cl}_2$  Solution) and IR Bands of Re(I)-dipyrinato Complexes

complex	absorption		emission			IR <sup>f</sup> CO modes ( $\text{cm}^{-1}$ )
	Abs. max. (nm)	$\lambda_{\text{max}}$ ( $\text{L mol}^{-1} \text{cm}^{-1}$ )	Em. Max (nm) <sup>d</sup>	$\Phi_{\text{em}}$	Stokes shift <sup>e</sup> ( $\text{cm}^{-1}$ )	
<b>1A</b>	487 <sup>a</sup>	33 800	708 <sup>b</sup>	<0.001 <sup>c</sup>	6410	1863, 1888, 2004
<b>2A</b>	491	36 600	706, 762	0.0014	6202	1880, 1913, 2015
<b>2B</b>	489	38 100	694, 755	0.0026	6041	1890, 1909, 2010
<b>2C</b>	488	37 700	694, 751	0.0060	6083	1883, 1910, 2013
<b>2D</b>	490	42 100	688, 754	0.0099	5873	1885, 1916, 2012
<b>2E</b>	490	40 500	691, 751	0.0051	5936	1881, 1912, 2011
<b>2F</b>	485	36 400	711, 764	<0.001 <sup>c</sup>	6554	1881, 1910, 2010
<b>3A</b>	480	25 500	no emission			1836, 1912
<b>3B</b>	481	27 300	no emission			1827, 1906
<b>3C</b>	481	25 400	no emission			1822, 1904
<b>3D</b>	487	27 600	706 <sup>b</sup>	<0.001 <sup>c</sup>	6370	1834, 1909
<b>3E</b>	481	27 200	no emission			1832, 1907
<b>3F</b>	474	40 900	no emission			1825, 1903
<b>3G</b>	474	32 200	no emission			1825, 1903
<b>4A</b>	472		not meas.			1834, 1914

<sup>a</sup>Recorded in DMSO. <sup>b</sup>Emission is very weak, and the long wavelength emission peak is not visible. <sup>c</sup>Emission was too weak to allow a more accurate estimation of the quantum yield. <sup>d</sup>The excitation wavelength was 485 nm for **1A**, **2A**–**E** and 480 nm for **2F** and **3D**. <sup>e</sup>The Stokes shifts are calculated using the absorption maximum and the high energy emission peak. <sup>f</sup>Measured in the solid state using ATR-IR spectroscopy.

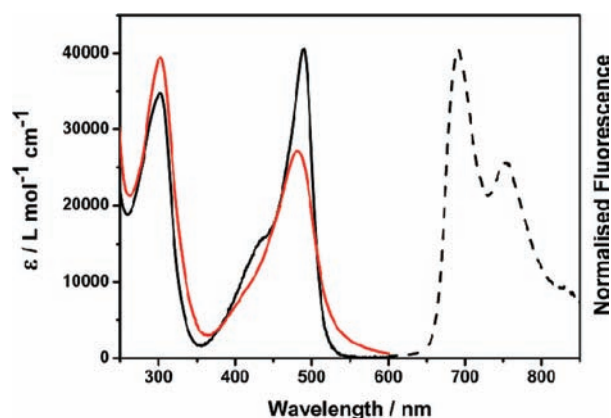


**Figure 6.** Absorption spectra of **2E** (black solid line) and **3E** (red solid line) and emission spectrum of **2E** (black dotted line,  $\lambda_{\text{ex}} = 485$  nm) in  $\text{CH}_2\text{Cl}_2$ .

transforming the complex from the ground state to the excited state in both Re(I) and Ru(II) complexes. The modes around 872 and 898  $\text{cm}^{-1}$ , which can be assigned as dipyrin (including the phenyl group) deformations, are enhanced for the Re(I) complexes relative to the Ru(II) complexes.

Although density functional theory (DFT) calculations suggest partial Re(I)-dipyrin metal-to-ligand charge-transfer (MLCT) character to the dominant electronic transition in the visible region (vide infra), no strong evidence for this is provided by the Raman spectra (where the CO vibrational modes, which are sensitive to changes at the Re center because of  $\pi$ -backbonding,<sup>21</sup> should be enhanced for  $\lambda_{\text{ex}} \approx 450$ –500 nm). Similar effects may also be evident if there was a standalone MLCT transition in this wavelength region. However, we note that relevant Raman peaks may be difficult to detect because of (i) the dependence of resonance Raman enhancements on the square of the oscillator strength of the corresponding electronic transition (the dipyrin  $\pi$ - $\pi^*$  transition has an oscillator strength four times greater than typical MLCT transitions), (ii) the limited extent of the MLCT character of the visible-wavelength absorption bands.

The emission properties of all the complexes in  $\text{CH}_2\text{Cl}_2$  were also investigated and the data are summarized in Table 2. Figure 6 displays the emission spectrum of **2E** as a

representative example. Upon excitation into the dipyrinato  $\pi$ - $\pi^*$  absorption band ( $\lambda_{\text{ex}} \sim 480$ –485 nm), a vibronically structured<sup>1d,3e</sup> emission profile was observed for the  $[\text{ReL}(\text{CO})_3\text{PR}_3]$  complexes, comprising an intense peak between 688 and 711 nm and a second, weaker peak between 751 and 762 nm. This equates to Stokes shifts in the vicinity of 6000  $\text{cm}^{-1}$ . The excitation spectrum of **2D** ( $\lambda_{\text{em}} = 700$  nm, Supporting Information, Figure S16b) displays peaks at 490 and 299 nm, which coincide with a dominant peak and a shoulder in the absorption spectrum. The excitation spectrum peak at 299 nm probably correlates with a dipyrinato  $S_0 \rightarrow S_2$  transition. On the other hand, the profile of the excitation spectrum in the region 250–300 nm differs considerably from the absorption spectrum, which indicates that some of the higher-energy electronic transitions do not result in luminescence. These transitions may be localized on regions of the complex that are electronically insulated from the dipyrin chromophore. All of the  $[\text{ReL}(\text{CO})_2(\text{PR}_3)(\text{PR}'_3)]$  complexes were nonemissive, except for **3D**, which exhibited very weak luminescence.

The emission quantum yields were determined to be between 0.0014 and 0.009 for the  $[\text{ReL}(\text{CO})_3\text{PR}_3]$  complexes at room temperature in deoxygenated  $\text{CH}_2\text{Cl}_2$  solution (Table 2). It has been established that one key nonradiative pathway for the relaxation of dipyrin-centered excited states involves the rotational motion of the *meso*-aryl group. Enhanced emission is observed where this motion is hindered,<sup>3c</sup> for example in mesityl dipyrin complexes,<sup>3a,e,18a</sup> and the relatively high quantum yield observed for **2D** complements these earlier studies. In a similar vein it is conceivable that the weak emission of **2F**, which has a  $\text{PBu}_3$  ligand, compared to the other complexes in this series, which have  $\text{PPh}_3$  ligands, stems from weaker (or nonexistent) noncovalent interactions between the *meso*-aryl groups of the dipyrins and the  $\text{PBu}_3$  ligand. The quantum yields of the  $[\text{ReL}(\text{CO})_3\text{PR}_3]$  complexes are similar to certain other dipyrin complexes<sup>3e</sup> but significantly lower than others.<sup>1d,e,m,3a,c,18a,22</sup> Re(I)-bipyridine complexes also typically have higher quantum yields.<sup>6d,f,23</sup>

The large Stokes shift is immediately suggestive of phosphorescence from a dipyrin-centered triplet excited electronic state, which is a relatively rare phenomenon in both dipyrinato complexes and BODIPYs.<sup>1d,3e,24</sup> Intersystem crossing from an initially formed singlet state is likely to be

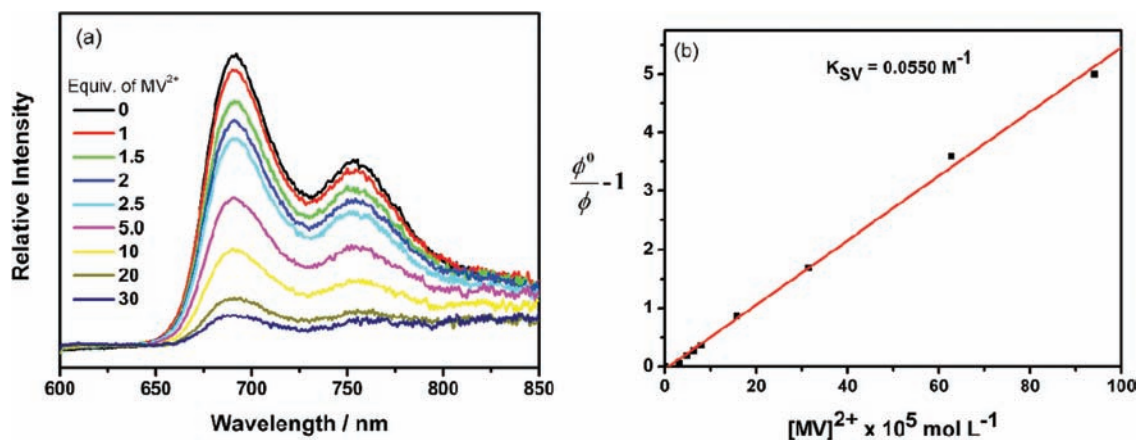


**Figure 7.** (a) Emission spectra of **2E** in  $\text{CH}_2\text{Cl}_2$  ( $\lambda_{\text{ex}} = 485$  nm) as a function of added methyl viologen ( $\text{MV}^{2+}$ , 1–30 mol equiv). (b) Stern–Volmer plot showing the quenching of emission from **2E** by  $\text{MV}^{2+}$ .  $\phi^0$  is the quantum yield in the absence of  $\text{MV}^{2+}$ , and  $\phi$  is the quantum yield in the presence of  $\text{MV}^{2+}$ .



promoted by the heavy atom effect.<sup>25</sup> This is supported by the dependence of the emission intensity on the presence of both dissolved oxygen<sup>26</sup> and methyl viologen ( $MV^{2+}$ ). Emission was brightest for rigorously degassed samples of **2A–E**; however, it was attenuated when air was bubbled through the solution (Supporting Information, Figure S16a). The controlled addition of  $MV^{2+}$  revealed that Stern–Volmer kinetics ( $K_{SV} = 0.055 \text{ M}^{-1}$ ) are obeyed for this quencher (Figure 7). It is also noteworthy that the two peaks in the emission spectrum are quenched at the same rate by  $MV^{2+}$ , which strongly implies that the peaks arise from the same excited state.  $MV^{2+}$  acts as a quencher by oxidizing the excited state of complexes **2A–E**. This is a promising observation in the context of employing these complexes for applications relying on photoinduced electron transfer, such such as the photocatalytic reduction of  $CO_2$  and dye-sensitized solar cells. Electron transfer from the excited state of dipyrinato complexes has been observed previously for covalent bis(dipyrinato)zinc(II)-fullerene<sup>27</sup> and porphyrin<sup>18b</sup> dyads. We found that reductive quenching of the excited state of **2E** by triethanolamine does not occur.

To characterize the frontier molecular orbitals of the  $[ReL(CO)_3PR_3]$  complexes, a DFT study of **2A** was undertaken. Preliminary results relevant to its optical properties are presented in the Supporting Information, Figure S22 and Table S1. The highest occupied molecular orbital (HOMO) and lowest unoccupied molecular orbital (LUMO) are confined on the dipyrinato ligand; predominantly the bispyrrolic core; however, the LUMO extends out to the *meso*-aryl ring (Supporting Information, Figure S22a). The HOMO-1 and HOMO-2 orbitals have mixed Re, CO, and dipyrinato ligand character, while the LUMO+1 orbital is restricted to the aryl ring of the dipyrinato ligand. Using time-dependent DFT (TD-DFT), a dominant transition ( $f = 0.340$ ) is predicted at 412 nm, which can be correlated with the intense peak in the experimental absorption spectrum at 491 nm. The HOMO, HOMO-2, and LUMO molecular orbitals are involved in this transition, and an electron density difference plot (Supporting Information, Figure S22b) indicates that the metal center loses electron density while the aryl ring gains electron density. There is also a reorganization of electron density on the bispyrrolic core. This picture is broadly consistent with a  $\pi-\pi^*$  designation for this transition, though it also has a significant degree of MLCT character. Similar observations have been made for a Re(I)-azadipyrinato complex.<sup>8</sup> The displacement of electron density on to the *meso*-aryl ring has also been predicted for a Ru(II)-dipyrinato complex.<sup>2b</sup> The suppression of the vibrational mode(s) that facilitate this electron density transfer, for example, by restricting aryl ring rotation as in **2D**, is thought to enhance the emissive properties of dipyrinato complexes.<sup>2b,3d</sup> Low energy transitions are predicted at 435 and 444 nm, but these are not apparent in the experimental absorption spectrum. Intriguingly, the predicted transition at 360 nm involves intraligand charge transfer on the dipyrinato chromophore, and this may contribute to the observed shoulder, which is generally attributed to vibronic effects, on the high-energy side of the  $\pi-\pi^*$  band.

#### Photochemical Ligand Substitution (PLS) Reactions.

We screened  $[ReL^A(CO)_3PR_3]$  for its propensity to undergo photochemical ligand substitution reactions and found (using both a mercury arc lamp and 515 nm, 488 nm, and 458 nm laser lines) that it is unaltered by visible light. This is an ideal characteristic in the context of applications in solar energy harvesting and conversion.

We did find that irradiation with a 355 nm pulsed laser in  $CD_3CN$  produced significant changes in its  $^1H$  and  $^{31}P$  NMR spectra (Figure 8, Supporting Information, Figures S17 and

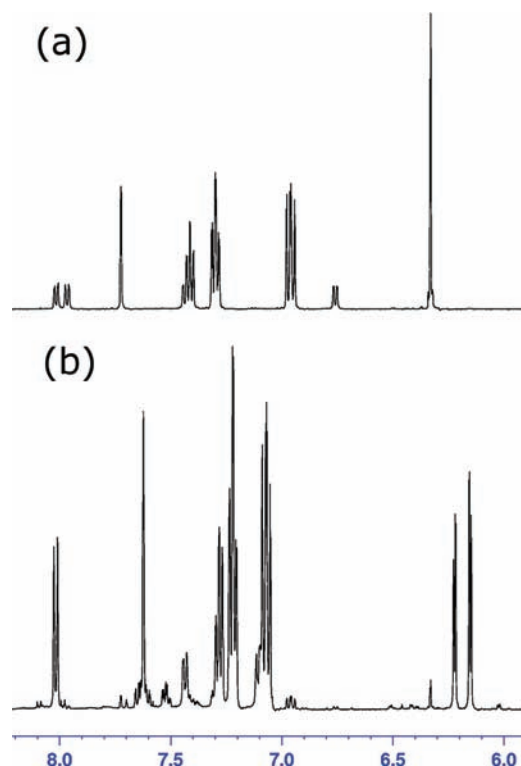


**Figure 8.** Aromatic region of the  $^1H$  NMR spectrum of **2A** (a) before and (b) after 2 h of irradiation with 355 nm laser light in  $CD_3CN$ .

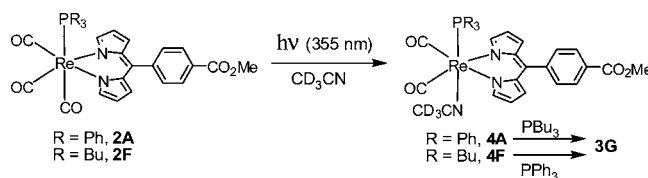


**Figure 9.** Irradiation of **2A** and **2F** with 355 nm laser light is proposed to generate complexes **4A** and **4F**, respectively. Further thermal reactions of **4A** with  $P(n-Bu)_3$  and **4F** with  $PPh_3$  produce complex **3G**.

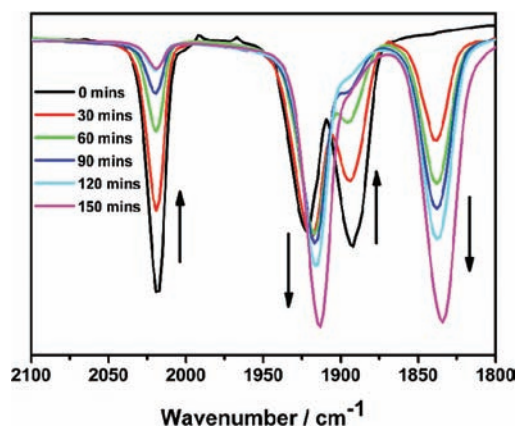


**Figure 10.** Photochemical conversion of **2A** to **4A** monitored by IR spectroscopy over a period of 150 min.



S18). After  $\sim 2.5$  h,  $>95\%$  of the starting material was consumed, and a clean spectrum corresponding to a new complex was evident (along with trace quantities of **3A**). Laser-induced *thermal* (rather than photochemical) processes can be ruled out on the basis of the low amount of power that is actually transferred to the sample and the fact that the temperature of the sample does not rise above  $30^\circ\text{C}$  during photolysis. We propose that the structure of the initially formed photolysis product is **4A** (Figure 9).  $^1\text{H}$  NMR,  $^{31}\text{P}$  NMR, 2D-COSY NMR (Supporting Information, Figures S17, S18, and S20) spectra support this conclusion by indicating that the  $\text{PPh}_3$  ligand remains coordinated and the dipyrin core retains its mirror symmetry. Although mass spectrometry proved fruitless, IR spectroscopy showed that the peaks corresponding to **2A** disappear, while peaks at  $1840\text{ cm}^{-1}$  and  $1920\text{ cm}^{-1}$  gradually grow into the spectrum (Figure 10). These are assigned as the out-of-phase totally symmetric and asymmetric vibrational modes of cis coordinated CO ligands, as expected for **4A**. Modest changes are evident in the electronic absorption spectrum (Supporting Information, Figure S21): the vibronic structure of the dominant absorption band of **2A** disappears, and this band broadens and shifts slightly to higher energy. When **2A** was irradiated in  $(\text{CD}_3)_2\text{CO}$ , a PLS reaction took place that also produced **3A**, though an intermediate complex analogous to **4A** could not be identified. Exhaustive attempts to isolate **4A** were made; however, it decomposes over a period of several days to give **2A**, **3A**, and one (or more) other unidentified compound(s) (Supporting Information, Figure S19). Presumably **2A** forms via a thermal reaction of **4A** with dissolved CO and **3A** results from a reaction with free  $\text{PPh}_3$ . This requisite free phosphine may arise from the decomposition of **4A**, which would also produce the unidentified material and free CO.

The PLS reaction of **2A** was repeated in the presence of free  $\text{PBu}_3$ . In this case, we anticipated that **4A** would form as an intermediate, and that it would subsequently react with  $\text{P}(n\text{-Bu})_3$  to yield complex **3G** (Figure 9). This reaction proceeds smoothly, and the characterization of **3G** produced in this manner was expedited by comparison with spectral data of independently prepared material. A PLS reaction also occurs if complex **2F** is irradiated in  $\text{CD}_3\text{CN}$ , and we assume that this yields **4F** (Figure 9). **3G** is formed when this PLS reaction is conducted in the presence of  $\text{PPh}_3$ .

PLS reactions have been well studied for  $\text{Re}(\text{I})$  complexes.<sup>6c,f,9c,11c,28</sup> Ligand labilization generally occurs from triplet metal-centered ( $^3\text{MC}$ ) excited states, which can be populated by internal conversion from MLCT excited states where a ligand such as bipy is coordinated to the metal center. In the case of  $\text{Re}(\text{I})$ -dipyrinato complexes such as **2A** and **2F**, suitable triplet excited states from which internal conversion to  $^3\text{MC}$  excited states could occur include the dipyrin-localized  $^3\pi-\pi^*$  state, a putative  $^3\text{MLCT}$  ( $\text{Re}/\text{dipyrin}$ ) state, and higher-energy dipyrin-based states. We have little information about the latter two, while the dipyrin-localized  $^3\pi-\pi^*$  state, which is believed to be responsible for the observed luminescence, probably lies far lower in energy than the  $^3\text{MC}$  states. In accord with this, no PLS was observed upon visible wavelength excitation.

An alternative to the above is the possibility that direct population of the  $^3\text{MC}$  states occurs. Although there is only very limited absorption by **2A** at  $355\text{ nm}$  (Figure 5,  $\epsilon = 1000\text{ M}^{-1}\text{ cm}^{-1}$ ), this is consistent with the low oscillator strengths of d-d transitions. The use of a pulsed laser as an intense light

source may compensate for the low efficiency of light absorption.

## CONCLUSION

The synthesis and characterization of the first  $\text{Re}(\text{I})$ -dipyrinato complexes with phosphine and CO coligands has been achieved. The complexes have prominent bands in the visible region of their absorption spectra which are ascribed primarily to a  $\pi-\pi^*$  transition centered on the dipyrinato ligand. For the  $[\text{ReL}(\text{CO})_3(\text{PR}_3)]$  family of complexes, excitation into this  $\pi-\pi^*$  band results in weak emission centered around  $700\text{ nm}$ . The large Stokes shift indicates phosphorescence from a triplet excited state. Intersystem crossing is probably facilitated by the heavy atom effect. Emission is quenched by the electron acceptor methyl viologen. The complexes are photostable toward visible irradiation; however, ligand substitution reactions can be induced with  $355\text{ nm}$  laser light. On the basis of their tunability, their ability to harvest visible light, their photostability, and the relatively high oxidation potential of their excited states, these complexes warrant further investigation as components of photochemical devices.

## ASSOCIATED CONTENT

### Supporting Information

Full experimental and characterization details, Raman spectra, and supplementary NMR, absorption and emission spectra. This material is available free of charge via the Internet at <http://pubs.acs.org>. CCDC 760501–760502 and 837651–837661 contain the supplementary crystallographic data for this paper. These data can be obtained free of charge from The Cambridge Crystallographic Data Centre via [www.ccdc.cam.ac.uk/data\\_request/cif](http://www.ccdc.cam.ac.uk/data_request/cif).

## AUTHOR INFORMATION

### Corresponding Author

\*E-mail: [s.telfer@massey.ac.nz](mailto:s.telfer@massey.ac.nz).

## ACKNOWLEDGMENTS

We thank Serena Smalley for establishing the synthetic protocol for  $\text{L}^{\text{F}}\text{H}$ , Professor Osamu Ishitani (Tokyo Institute of Technology) for valuable discussions, and Dr. Patrick Edwards (Massey University) for expert assistance with NMR spectra

## REFERENCES

- (1) (a) Wood, T. E.; Thompson, A. *Chem. Rev.* **2007**, *107*, 1831. (b) Yadav, M.; Singh, A. K.; Maiti, B.; Pandey, D. S. *Inorg. Chem.* **2009**, *48*, 7593. (c) Yadav, M.; Kumar, P.; Pandey, D. S. *Polyhedron* **2010**, *29*, 791. (d) Hanson, K.; Tamayo, A.; Diev, V. V.; Whited, M. T.; Djurovich, P. I.; Thompson, M. E. *Inorg. Chem.* **2010**, *49*, 6077. (e) Kobayashi, J.; Kushida, T.; Kawashima, T. *J. Am. Chem. Soc.* **2009**, *131*, 10836. (f) Maeda, H.; Hashimoto, T. *Chem.—Eur. J.* **2007**, *13*, 7900. (g) Salazar-Mendoza, D.; Baudron, S. A.; Hosseini, M. W. *Inorg. Chem.* **2008**, *47*, 766. (h) Baudron, S. A. *CrystEngComm* **2010**, *12*, 2288. (i) Bronner, C.; Baudron, S. A.; Hosseini, M. W. *Inorg. Chem.* **2010**, *49*, 8659. (j) King, E. R.; Betley, T. A. *Inorg. Chem.* **2009**, *48*, 2361. (k) Scharf, A. B.; Betley, T. A. *Inorg. Chem.* **2011**, *50*, 6837. (l) King, E. R.; Hennessy, E. T.; Betley, T. A. *J. Am. Chem. Soc.* **2011**, *133*, 4917. (m) Filatov, M. A.; Lebedev, A. Y.; Mukhin, S. N.; Vinogradov, S. A.; Cheprakov, A. V. *J. Am. Chem. Soc.* **2010**, *132*, 9552. (n) Ma, L.; Shin, J.-Y.; Patrick, B. O.; Dolphin, D. *CrystEngComm* **2008**, *10*, 1531. (o) Crawford, S. M.; Al-Sheikh Ali, A.; Cameron, T. S.; Thompson, A. *Inorg. Chem.* **2011**, *50* (17), 8207–8213.

- (2) (a) Hall, J. D.; McLean, T. M.; Smalley, S. J.; Waterland, M. R.; Telfer, S. G. *Dalton Trans.* **2010**, 39, 437. (b) Telfer, S. G.; McLean, T. M.; Waterland, M. R. *Dalton Trans.* **2011**, 40, 3097.
- (3) (a) Thoi, V. S.; Stork, J. R.; Magde, D.; Cohen, S. M. *Inorg. Chem.* **2006**, 45, 10688. (b) Ikeda, C.; Ueda, S.; Nabeshima, T. *Chem. Commun.* **2009**, 2544. (c) Sutton, J. M.; Rogerson, E.; Wilson, C. J.; Sparke, A. E.; Archibald, S. J.; Boyle, R. W. *Chem. Commun.* **2004**, 1328. (d) Sazanovich, I. V.; Kirmaier, C.; Hindin, E.; Yu, L.; Bocian, D. F.; Lindsey, J. S.; Holten, D. J. *Am. Chem. Soc.* **2004**, 126, 2664. (e) Bronner, C.; Baudron, S. A.; Hosseini, M. W.; Strassert, C. A.; Guenet, A.; De Cola, L. *Dalton Trans.* **2010**, 39, 180.
- (4) (a) Ulrich, G.; Ziesel, R.; Harriman, A. *Angew. Chem., Int. Edit.* **2008**, 47, 1184. (b) Loudet, A.; Burgess, K. *Chem. Rev.* **2007**, 107, 4891. (c) Bañuelos, J.; Martín, V.; Gómez-Durán, C. F. A.; Córdoba, I. J. A.; Peña-Cabrera, E.; García-Moreno, I.; Costela, Á.; Pérez-Ojeda, M. E.; Arbeloa, T.; Arbeloa, Í. L. *Chem.—Eur. J.* **2011**, 17, 7261.
- (5) (a) Takeda, H.; Ishitani, O. *Coord. Chem. Rev.* **2010**, 254, 346. (b) Takeda, H.; Koike, K.; Inoue, H.; Ishitani, O. *J. Am. Chem. Soc.* **2008**, 130, 2023. (c) Ettetdgui, J.; Diskin-Posner, Y.; Weiner, L.; Neumann, R. *J. Am. Chem. Soc.* **2011**, 133, 188. (d) Morris, A. J.; Meyer, G. J.; Fujita, E. *Acc. Chem. Res.* **2009**, 42, 1983. (e) Takeda, H.; Ohashi, M.; Tani, T.; Ishitani, O.; Inagaki, S. *Inorg. Chem.* **2010**, 49, 4554. (f) Koike, K.; Naito, S.; Sato, S.; Tamaki, Y.; Ishitani, O. *J. Photochem. Photobiol., A* **2009**, 207, 109. (g) Sato, S.; Koike, K.; Inoue, H.; Ishitani, O. *Photochem. Photobiol. Sci.* **2007**, 6, 454.
- (6) (a) Smithback, J. L.; Helms, J. B.; Schutte, E.; Woessner, S. M.; Sullivan, B. P. *Inorg. Chem.* **2006**, 45, 2163. (b) Wrighton, M.; Morse, D. L. *J. Am. Chem. Soc.* **1974**, 96, 998. (c) Koike, K.; Okoshi, N.; Hori, H.; Takeuchi, K.; Ishitani, O.; Tsubaki, H.; Clark, I. P.; George, M. W.; Johnson, F. P. A.; Turner, J. J. *J. Am. Chem. Soc.* **2002**, 124, 11448. (d) Hori, H.; Koike, K.; Ishizuka, M.; Takeuchi, K.; Ibusuki, T.; Ishitani, O. *J. Organomet. Chem.* **1997**, 530, 169. (e) Giordano, P. J.; Wrighton, M. S. *J. Am. Chem. Soc.* **1979**, 101, 2888. (f) Koike, K.; Tanabe, J.; Toyama, S.; Tsubaki, H.; Sakamoto, K.; Westwell, J. R.; Johnson, F. P. A.; Hori, H.; Saitoh, H.; Ishitani, O. *Inorg. Chem.* **2000**, 39, 2777. (g) Lo, K. K.-W.; Zhang, K. Y.; Li, S. P.-Y. *Eur. J. Inorg. Chem.* **2011**, 2011, 3551.
- (7) Ziesel, R.; Harriman, A. *Chem. Commun.* **2011**, 47, 611.
- (8) Partyka, D. V.; Deligonul, N.; Washington, M. P.; Gray, T. G. *Organometallics* **2009**, 28, 5837.
- (9) (a) Caspar, J. V.; Meyer, T. J. *J. Phys. Chem.* **1983**, 87, 952. (b) Worl, L. A.; Duesing, R.; Chen, P. Y.; Dellaciana, L.; Meyer, T. J. *J. Chem. Soc., Dalton Trans.* **1991**, 849. (c) Sato, S.; Sekine, A.; Ohashi, Y.; Ishitani, O.; Blanco-Rodriguez, A. M.; Vicek, A.; Unno, T.; Koike, K. *Inorg. Chem.* **2007**, 46, 3531.
- (10) (a) Hori, H.; Johnson, F. P. A.; Koike, K.; Ishitani, O.; Ibusuki, T. *J. Photochem. Photobiol., A* **1996**, 96, 171. (b) Tsubaki, H.; Tohyama, S.; Koike, K.; Saitoh, H.; Ishitani, O. *Dalton Trans.* **2005**, 385.
- (11) (a) Caspar, J. V.; Sullivan, B. P.; Meyer, T. J. *Inorg. Chem.* **1984**, 23, 2104. (b) Schutte, E.; Helms, J. B.; Woessner, S. M.; Bowen, J.; Sullivan, B. P. *Inorg. Chem.* **1998**, 37, 2618. (c) Pac, C. J.; Kaseda, S.; Ishii, K.; Yanagida, S. *J. Chem. Soc., Chem. Commun.* **1991**, 787.
- (12) (a) Telfer, S. G.; Wuest, J. D. *Cryst. Growth Des.* **2009**, 9, 1923. (b) Fergusson, J. E.; March, F. C.; Couch, D. A.; Emerson, K.; Robinson, W. T. *J. Chem. Soc. A* **1971**, 440.
- (13) (a) Kilduff, B.; Pogozhev, D.; Baudron, S. A.; Hosseini, M. W. *Inorg. Chem.* **2010**, 49, 11231. (b) Maeda, H.; Hashimoto, T.; Fujii, R.; Hasegawa, M. *J. Nanosci. Nanotechnol.* **2009**, 9, 240.
- (14) Sullivan, B. P.; Meyer, T. J. *J. Chem. Soc., Chem. Commun.* **1984**, 1244.
- (15) Vlcek, A. In *Photophysics of Organometallics*; Springer: Heidelberg, Germany, 2010; Vol. 29, p 73.
- (16) (a) McLean, T. M.; Cleland, D. M.; Lind, S. J.; Gordon, K. C.; Telfer, S. G.; Waterland, M. R. *Chem.—Asian J.* **2010**, 5, 2036. (b) Smalley, S. J.; Waterland, M. R.; Telfer, S. G. *Inorg. Chem.* **2009**, 48, 13.
- (17) Brückner, C.; Karunaratne, V.; Rettig, S. J.; Dolphin, D. *Can. J. Chem.* **1996**, 74, 2182.
- (18) (a) Sazanovich, I. V.; Kirmaier, C.; Hindin, E.; Yu, L. H.; Bocian, D. F.; Lindsey, J. S.; Holten, D. J. *Am. Chem. Soc.* **2004**, 126, 2664. (b) Yu, L.; Muthukumar, K.; Sazanovich, I. V.; Kirmaier, C.; Hindin, E.; Diers, J. R.; Boyle, P. D.; Bocian, D. F.; Holten, D.; Lindsey, J. S. *Inorg. Chem.* **2003**, 42, 6629.
- (19) (a) Arbeloa, T. L.; Arbeloa, F. L.; Arbeloa, I. L.; García-Moreno, I.; Costela, A.; Sastre, R.; Amat-Guerri, F. *Chem. Phys. Lett.* **1999**, 299, 315. (b) Kee, H. L.; Kirmaier, C.; Yu, L.; Thamyongkit, P.; Youngblood, W. J.; Calder, M. E.; Ramos, L.; Noll, B. C.; Bocian, D. F.; Scheidt, W. R.; Birge, R. R.; Lindsey, J. S.; Holten, D. J. *Phys. Chem. B* **2005**, 109, 20433.
- (20) Lager, E.; Liu, J.; Aguilar-Aguilar, A.; Tang, B. Z.; Pena-Cabrera, E. *J. Org. Chem.* **2009**, 74, 2053.
- (21) Waterland, M. R.; Simpson, T. J.; Gordon, K. C.; Burrell, A. K. *J. Chem. Soc., Dalton Trans.* **1998**, 185.
- (22) Sakamoto, N.; Ikeda, C.; Yamamura, M.; Nabeshima, T. *J. Am. Chem. Soc.* **2011**, 133, 4726.
- (23) Tsubaki, H.; Sekine, A.; Ohashi, Y.; Koike, K.; Takeda, H.; Ishitani, O. *J. Am. Chem. Soc.* **2005**, 127, 15544.
- (24) (a) Sabatini, R. P.; McCormick, T. M.; Lazarides, T.; Wilson, K. C.; Eisenberg, R.; McCamant, D. W. *J. Phys. Chem. Lett.* **2011**, 2, 223. (b) Nastasi, F.; Puntoriero, F.; Campagna, S.; Diring, S.; Ziesel, R. *Phys. Chem. Chem. Phys.* **2008**, 10, 3982. (c) Harriman, A.; Rostron, J. P.; Cesario, M. I.; Ulrich, G.; Ziesel, R. *J. Phys. Chem. A* **2006**, 110, 7994.
- (25) McGlynn, S. P.; Azumi, T.; Kinoshita, M. *Molecular Spectroscopy of the Triplet State*; Prentice-Hall: Englewood Cliffs, NJ, 1969.
- (26) Lakowicz, J. R. *Principles of Fluorescence Spectroscopy*, 3rd ed.; Springer: New York, 2006.
- (27) Rio, Y.; Sánchez-García, D.; Seitz, W.; Torres, T.; Sessler, J. L.; Guldi, D. M. *Chem.—Eur. J.* **2009**, 15, 3956.
- (28) (a) Sato, S.; Morimoto, T.; Ishitani, O. *Inorg. Chem.* **2007**, 46, 9051. (b) Kumar, A.; Sun, S. S.; Lees, A. J. In *Topics in Organometallic Chemistry*; Springer-Verlag: Berlin, 2010; Vol. 29, p 1; (c) Kirgan, R. A.; Sullivan, B. P.; Rillema, D. P. In *Photochemistry and Photophysics of Coordination Compounds II*; Springer: Berlin, Germany, 2007; Vol. 281, p 45.